JOURNAL OF PROPULSION AND POWER
Vol. 22, No. 6, November–December 2006

Vaporization Lengths of Hydrazine Fuels Burning with NTO

Cesar A. V. Salvador* and Fernando S. Costa†
National Space Research Institute, 12630-000 Cachoeira Paulista, Brazil

DOI: 10.2514/1.18348

The performances of single hydrazines and hydrazine mixtures burning with NTO in a bipropellant rocket combustion chamber are compared. Systems using single hydrazines (N_2H_4, MMH, UDMH) and hydrazine mixtures (MMH/N_2H_4 and $UDMH/N_2H_4$) were simulated with total mass flow rates of 45.29 g/s and 89.25 g/s, respectively, in a chamber with diameter 40 mm. A one-dimensional mathematical model was developed, assuming that combustion and turbulent mixture processes are controlled by droplet vaporization, and that droplet diameters follow the Rosin–Rammler distribution function with a finite number of diameters. The effects of drag, thermal expansion, transient vaporization, and heat transfer by convection and radiation to the droplets and to the chamber walls were considered. The influences of chamber pressure, equivalence ratio, initial gas temperature, number of size classes, Sauter mean diameter, and parameters of the Rosin–Rammler distributions on vaporization lengths of droplets are analyzed. Profiles of normalized diameters, temperatures, velocities, heat losses, vaporization rates, and other flow properties along the chamber are described.

Nomenclature

A = area or constant of Antoine's equation
B = constant of Antoine's equation
B_M = transfer number
C = constant of Antoine's equation
C_D = drag coefficient
C_p = specific heat at constant pressure
D = diameter
D_{32} = Sauter mean diameter
F = drag
f = mixture ratio
h = specific enthalpy
h_{fg} = vaporization enthalpy
$\hat{h}^*$ = convection coefficient for droplet heating
$\hat{h}_g$ = convection coefficient for wall heating
$\bar{M}$ = average molar mass
m_d = droplet mass
$\dot{m}$ = mass flow rate
$\dot{m}_v$ = vaporization rate
N = number of droplet size classes
Nu_0 = Nusselt number for heat transfer around a solid sphere
P = pressure
P_c = critical pressure
P_v = vapor pressure at droplet surface
Pr = Prandtl number
Q = volume fraction of droplets
$\dot{Q}$ = heat flow
q = Rosin–Rammler parameter
R_0 = universal constant of gases
Re = Reynolds number
T = temperature
T_b = boiling temperature
V_c = critical volume
v = velocity
v_{rel} = relative velocity droplet-gas
We = Weber number
Y_s = mass fraction of water vapor at droplet surface
ε = emissivity
η = viscosity
λ = conductivity
ρ = density
σ = Stefan–Boltzmann constant
τ = surface tension
Φ = equivalence ratio

Subscripts

c = combustion chamber or denotes critical condition
cond = conduction
conv = convection
d = droplet
F = fuel
g = gas
i = species or size class of fuel
j = species or size class of oxidizer
l = liquid or droplet
Ox = oxidizer
P = premixed
p = product, fuel component
q = oxidant component
r = reference condition
rad = radiation
s = stoichiometric or droplet surface
T = total
v = vapor
w = wall
0 = injection position
∞ = conditions away from chamber

I. Introduction

LIQUID propellants are commonly used in rocket launchers because of their high specific impulses, high thrust levels, and better thrust control as compared with solid propellants. In bipropellant systems, an oxidizer and a fuel are stored in separate reservoirs and later are vaporized, mixed, ignited, and burned inside the rocket combustion chamber. In general, propellants require the use of igniters, such as pyrotechnical and spark ignition systems; nevertheless there are propellants that react spontaneously when in contact, called hypergolic propellants. Examples of common oxidizers used in rockets include LO_2, NTO (N_2O_4, nitrogen tetroxide), HNO_3, and H_2O_2, and examples of fuels are N_2H_4

Received 27 June 2005; revision received 7 February 2006; accepted for publication 8 February 2006.

*Graduate student, LCP/INPE, Rod. Presidente Dutra, km 40.
†Researcher, LCP/INPE, Rod. Presidente Dutra, km 40.

(hydrazine), UDMH (unsymmetrical dimethyl hydrazine), MMH (monomethyl hydrazine), LH_2, and kerosene.

Hydrazine and its derivatives (UDMH and MMH) and NTO are hypergolic propellants, presenting good performance when compared with other common fuels. They can be used in launchers, using a single start, or in thrusters for attitude control, maneuvering, and orbit transfer, that require constant restarts.

Mixtures of hydrazine and its derivatives, e.g., N_2H_4/UDMH and N_2H_4/MMH, burning with NTO are often used. UDMH is more stable than N_2H_4 and MMH, especially in high temperatures; however, it yields a lower specific impulse. MMH has better shock resistance, better thermal properties, and larger temperature range in liquid phase than hydrazine. In thrusters with regenerative cooling, using hydrazine or mixtures of its derivatives, additives can be used to reduce its freezing point and to increase the heat transfer along the chamber walls, avoiding freezing of the liquid inside the ducts [1].

Hydrazine mixtures with UDMH, called aerozines, are used with a proportion of 50–70% in mass of N_2H_4, to decrease the freezing point of hydrazine. Additional characteristics and descriptions of applications of hydrazine and its derivatives are presented in [1].

Mathematical models of spray combustion are important to the project and development of rocket combustion chambers. The use of these models allows to reduce the number of tests in prototypes, to make improvements in the project, or to modify operational conditions of combustion chambers, at a lower cost and in shorter time than using empirical or try and error methods. There are several models available in the literature describing the combustion of sprays. They can be classified [2] in locally homogeneous flow models (LHF), in separated flow models (SF), and models based on experimental correlations (EC).

EC models are simpler to use, but require a large number of experiments in a given combustion chamber and only can be used in combustors of the same type.

LHF models consider the spray equivalent to a single phase flow where the liquid and gas phases are in dynamic and thermodynamic equilibrium, with the same velocities and temperatures in each point of the flow. The basic hypothesis is that the variations in flow properties are slower than the transport of mass, energy, and momentum among the phases. The LHF models are useful for sprays with very small droplets, bubble flows, and sprays in supercritical conditions. The initial distributions of velocity and droplet sizes are not necessary and, therefore, little information is required about the injector. Another advantage of LHF models is that the calculations are not so complex neither require as much time as SF models. The existent one-phase flow models can be used with little modifications to represent LHF models. Less empirical constants are required in the LHF than in the SF models. SF models take into account the transport processes in the liquid and gas phases, and the transport of mass, momentum, and energy among the phases. The common practice is to use empirical expressions for the drag and for the heat and mass transfer of the droplets, because the detailed modeling of the flow around each droplet would require a very large computational time.

Spray models can also be classified as 0, 1, 2, or 3-D models, depending on the number of space dimensions considered, or can be classified in steady state or transient models, whether time variations are considered or not.

Zero and one-dimensional models have been used frequently in the design of rocket nozzles and chambers. In 1-D models, the flow properties depend only on one space coordinate. Because mass, momentum, and energy balances have to be satisfied at each chamber section, 1-D models calculate approximate average values and properties at each chamber section. These models are the most used due to their simplicity and reduced time of computation; however, they can involve various details of the vaporization and burning process of the droplets [3–11].

It should be noted that 2-D and 3-D models allow a more detailed description of the reactive flow inside the chamber than 1-D models and, at principle, would provide a better performance prediction. However it is extremely difficult to determine experimentally the detailed 3-D characteristics of the two-phase flow inside a rocket combustion chamber. The modeling of each phenomenon involved, such as injection, liquid jet breakup, droplet vaporization, turbulent mixing, and turbulent combustion, includes approximations that summed up can eventually lead to larger errors than in 1-D models, if the assumptions adopted in the 1-D models are properly made and are consistent with experimental data.

To compare the performance of hydrazine fuels, and its mixtures, burning with NTO, a 1-D spray vaporization and combustion model was developed to simulate a multipropellant rocket combustion chamber. It was assumed that the combustion process is controlled by droplet vaporization, i.e., the burning and turbulent mixing rates are considered much faster than the droplet vaporization rates. The droplet size distributions of the liquid propellants follow the Rosin–Rammler model with a finite number of diameters. The effects of drag, thermal expansion, transient heating and vaporization, convection and radiation to the droplets, and heat losses to the chamber walls are considered. Effects of droplet deformation on drag coefficients are considered. The model is described in detail in [12], and is based on previous models [8,10].

The influences of the chamber pressure, equivalence ratio, initial gas temperature, number of size classes of droplets, parameters of the Rosin–Rammler distribution, and Sauter mean diameter on the distance for complete vaporization of drops are analyzed. The profiles of normalized diameters, temperatures, velocities, heat losses, vaporization rates of the drops, and other properties of the flow along the chamber are described. Numerical results for multipropellant systems using mixtures of N_2H_4/UDMH and N_2H_4/MMH with NTO are also presented.

The model determines qualitatively the effects of pressure and other variables on vaporization lengths of hydrazine sprays and their mixtures. In general, the design of rocket combustion chambers is based on characteristic lengths, L^* = chamber volume/throat area, derived from experimental data. In the case of hydrazines the characteristic lengths vary from 30 to 35 in [13].

A main feature of the present model is the ability to determine an appropriate number of droplet size classes using the Rosin–Rammler distribution function, thus allowing to obtain a reasonable estimate of the vaporization length of a bipropellant spray for several conditions. The model considers variable thermodynamic properties, such as heats of vaporization of droplets dependent on pressure and temperature. This increases the accuracy of the model as compared with other models, even in supercritical pressures. The software was written in the MATLAB 6.5 language with a simple and versatile interface that can be used for any combination of liquid propellants with known thermodynamic and transport properties.

II. Mathematical Model

A scheme of the reactive process inside a bipropellant combustion chamber is depicted in Fig. 1. The fuel(s) and the oxidizer(s) are injected into the combustion chamber through an injection plate, forming liquid jets that break up immediately generating sprays with known droplet diameter distributions. The droplets enter in contact with the hot combustion products, vaporize, and form fuel and oxidizer vapors which mix and change the local equivalence ratio. The mixture burns instantaneously, modifying the temperature and composition of the combustion products. It is assumed that fractions

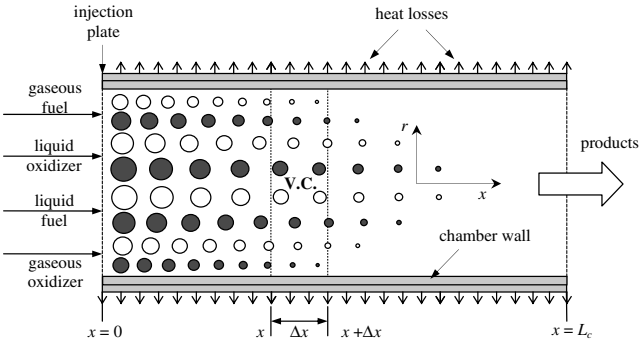

Fig. 1 Scheme of 1-D bipropellant spray vaporization and combustion inside a rocket chamber.

of fuel and oxidizer are injected as gases, to create a gaseous flow near the injection plate, corresponding to recirculating flows in real systems. Several factors such as gas recirculation, high gas velocities, injection configuration, chamber geometry, impinging of liquid jets, and flow with different phase velocities produce intense turbulent mixing, which makes the droplet vaporization rates a controlling factor.

Because turbulent mixture and combustion are fast compared to vaporization, the gas composition is calculated at each section for an equilibrium process at constant pressure and constant temperature, however, considering the heat transfer from the gas mixture to the chamber walls and to the droplets. Pressure is approximately constant along the chamber, whereas the gas temperature varies significantly, depending on the equivalence ratio of the gas mixture.

The model considers that droplet diameters of fuel(s) and oxidizer (s) are described by Rosin–Rammler distribution functions whose parameters can be obtained experimentally and vary with injector type. The model takes into account the transient vaporization, according to the methodology presented by Chin and Lefebvre [14]. The droplet vaporization during the transient phase can be significant, and depends on the gas mixture thermodynamic properties. Droplet thermal expansion is considered during the heating phase until the droplet attains an equilibrium temperature, or "wet bulb" temperature, when the droplet diameter starts to decrease continuously.

The gases and droplets present different initial velocities, but, as vaporization proceeds, the relative velocity between droplets and gas mixture tends to zero. The effects of droplet deformation on drag are considered; nevertheless droplet breakup and collisions are neglected.

A. Equations of the Problem

Equations of the problem are obtained considering volume elements of thickness Δx along the chamber, as indicated in Fig. 2. Mass and energy balances are made in these elements, yielding a set of ordinary differential equations which can be numerically integrated once the initial conditions are known. An analysis of the momentum fluxes shows that the pressure is approximately constant along the chamber.

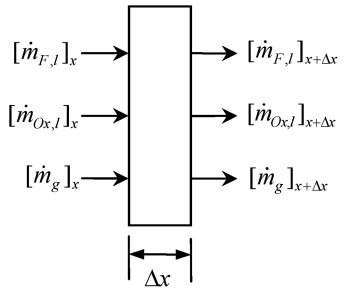

a) Mass conservation

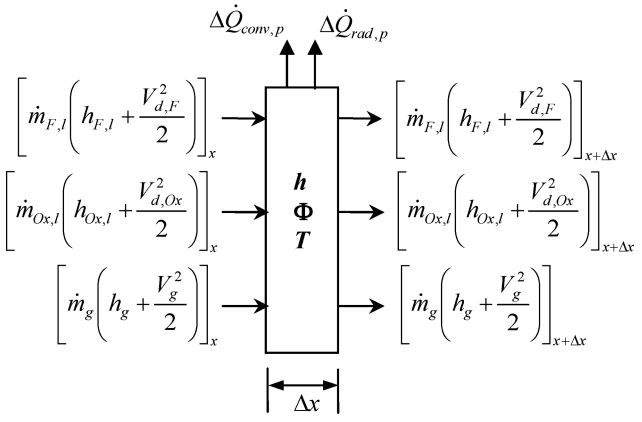

b) Energy conservation

Fig. 2 Volume elements for mass and energy balances.

B. Distribution of Droplet Diameters

The Rosin–Rammler distribution function was adopted to describe the distribution of droplet diameters. It can be written in terms of the cumulative volume fraction [15]:

$$Q = 1 - \exp\left[-\left(\frac{D}{X}\right)^q\right] \tag{1}$$

where Q is the volume fraction of the spray containing droplets of diameter less than D, and q and X are constants. The parameter q measures the spray uniformity: when q increases the spray becomes more uniform, and if q is infinite, then all droplets have the same diameter. According to Lefebvre [15], in most sprays q is between 1.5 and 4. The constant X represents a spray characteristic diameter that depends on the problem considered. For combustion applications, X is linked to parameter q by relation [15]:

$$X = D_{32}\left[\Gamma\left(1 - \frac{1}{q}\right)\right] \tag{2}$$

where Γ is the gamma function and D_{32} is the Sauter mean diameter (SMD), defined by

$$D_{32} = \frac{\sum N_k D_k^3}{\sum N_k D_k^2} \tag{3}$$

where N_k is the number of droplets having diameter D_k in the spray. The SMD represents an average droplet diameter, proportional to the ratio of total volume and total surface area of all spray droplets, and its value depends on injector type, liquid properties, and exit conditions of the spray.

In the present model a finite number of droplet class sizes is considered. Each class includes droplets within a given range of diameters, for example, 0–60, 60–120, 120–180, and 180–240 μm. To simplify the analysis each class is characterized by a representative SMD. The procedure for obtaining the representative SMD of a droplet size class is described in [12]. A maximum droplet diameter, $D_{\max}$, is calculated for the different Rosin–Rammler distributions of fuels and oxidizers, above which the propellant volume percentage is less than 0.1%. Therefore, droplets with diameter larger than $D_{\max}$ are not considered.

Figure 3 shows the influence of the number of size classes on the Rosin–Rammler distribution for $D_{32} = 25$ μm and $q = 1.5$ using MMH and NTO with data from Table 1. An increase in the number of size classes to represent the diameter distribution can produce more accurate results; however, it increases the time of computation. Figure 4a shows that above four size classes there is no significant change of the vaporization length, especially for pressures higher than 5 atm for MMH and NTO. Figure 4b shows the influence of the Rosin–Rammler parameters q and D_{32} on $D_{\max}$ for $q = 1.5$, 2.0, 2.5, 3.0 and $D_{32} = 25, 50, 75$ μm. If D_{32} is kept constant, an increase in q decreases $D_{\max}$, because the spray becomes more uniform with droplets having diameter close to D_{32}, as mentioned before. On the other hand, when q is kept constant, an increase of D_{32} increases $D_{\max}$, a consequence of the higher probability of existing larger droplets, as given by Eq. (1).

C. Mass Balance

Figure 2a shows the mass flow rates of the liquid and gas phases entering and exiting a volume element or control volume (CV). Making the balance of these rates, it yields

$$\dot{m}'_g + \dot{m}'_{F,l} + \dot{m}'_{\mathrm{Ox},l} = 0 \tag{4}$$

where the superscript $'$ denotes derivative with respect to x.

The derivative of the total mass of each propellant is function of the partial mass flow rates of each droplet size class:

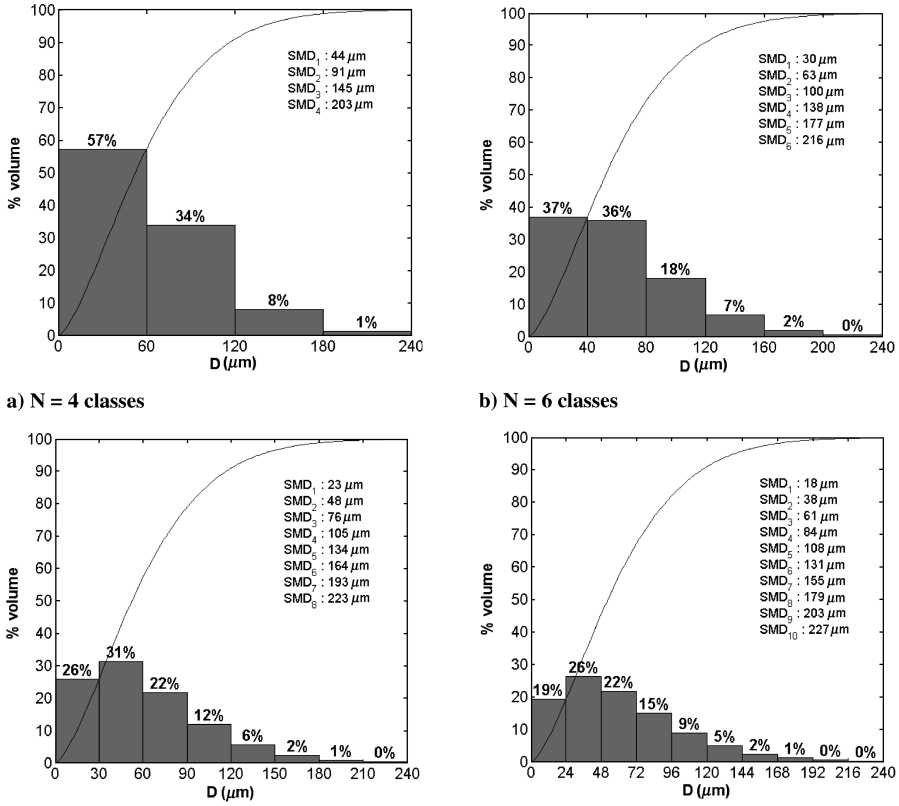

a) N = 4 classes **b) N = 6 classes**

c) N = 8 classes **d) N = 10 classes**

Fig. 3 Influence of the number of size classes on Rosin–Rammler distribution function.

$$\dot{m}'_{F,l} = \sum_{p=1}^{\mathrm{NF}} \sum_{i=1}^{I} \dot{m}'_{F,p,l,i} \tag{5a}$$

$$\dot{m}'_{\mathrm{Ox},l} = \sum_{q=1}^{\mathrm{NO}} \sum_{j=1}^{J} \dot{m}'_{\mathrm{Ox},q,l,j} \tag{5b}$$

where I and J indicate the total number of size classes of fuel and oxidizer, respectively, and NF and NO are the numbers of different fuels and oxidizers injected, respectively. It should be noted that the total mass flow of each propellant is divided in several partial mass flow rates corresponding to the number of size classes chosen.

The partial mass flow rates of each propellant are calculated by multiplying the volume fraction of droplets inside a droplet size class i or j by the total mass flow rate, following the discrete Rosin–Rammler distribution. Because liquid density is the same for all droplets at the injection plane, the volume fractions can be used instead of mass fractions.

Equation (4) can be integrated along x to obtain an expression for the mass flow rate of gas crossing a given axial position, $\dot{m}_{g,x}$:

$$\dot{m}_{g,x} = \dot{m}_{g,0} + (\dot{m}_{F,l,0} - \dot{m}_{F,l,x}) + (\dot{m}_{\mathrm{Ox},l,0} - \dot{m}_{\mathrm{Ox},l,x}) \tag{6}$$

where subscripts 0 and x indicate conditions at injection and at an arbitrary axial position, respectively.

Table 1 Constants of Antoine and Haggenmacher equations[a]

Species	NTO	N_2H_4	MMH	UDMH
T, K	264–321	270–653	275–567	275–522
A	8.2431	6.8413	6.4899	6.7474
B	1921.8	1594	1354.9	1478.9
C	13.788	−57.383	−59.3457	−25.3076

[a]Data from [1,16].

The mass flow rates of each size class of droplets of fuel and oxidizer are, respectively,

$$\dot{m}_{F,l,i,0} = \sum_{p=1}^{\mathrm{NF}} \rho_{F,p,l,i,0} A_{F,p,l,i,0} v_{d,F,p,i,0}, \qquad i = 1, \ldots, I \tag{7a}$$

$$\dot{m}_{\mathrm{Ox},l,j,0} = \sum_{q=1}^{\mathrm{NO}} \rho_{\mathrm{Ox},q,l,j,0} A_{\mathrm{Ox},q,l,j,0} v_{d,\mathrm{Ox},q,j,0}, \qquad j = 1, \ldots, J \tag{7b}$$

where $\rho_{F,p,l,i,0}$ and $\rho_{\mathrm{Ox},q,l,j,0}$ are the liquid fuel and oxidizer densities, $v_{d,F,p,i,0}$ and $v_{d,\mathrm{Ox},q,j,0}$ are the fuel and oxidizer droplet velocities, and $A_{F,p,l,i,0}$ and $A_{\mathrm{Ox},q,l,j,0}$ are the partial injection areas ($x = 0$) corresponding to the droplet size classes of fuel and oxidizer, respectively. The partial area of each droplet size class, i or j, is calculated by multiplying its volume percentage by the total area, assuming that all droplets coming out from an injector hole have the same density and velocity.

The liquid or droplet temperature at injection is specified for each propellant. It is assumed the same for all size classes, but it depends on tank temperature and injection velocity. The liquid density is a known parameter which depends on the liquid temperature at injection. The total area for each propellant (exit area of liquid in the injector) is also a known parameter and depends on the injector type. It can be calculated using the diameter of the liquid jet. In general, the injectors have more than one exit channel, and, therefore, the total area is the sum of all individual areas. The breakup distance depends on the injector type and injection geometry. For impinging jets, the breakup distance is about the impinging point distance. For a single liquid jet it is a few times the diameter of the injection hole, being usually much smaller than the vaporization length.

The mass flow rate of liquid for each propellant is a known value, specified in terms of thrust level and desired operational conditions. Assuming that injection velocities of all droplet size classes are the same, they can be calculated as

$$v_{d,F,p,0} = \dot{m}_{F,p,l,0}/(\rho_{F,p,l,0}A_{F,p,l,0}) \tag{8a}$$

$$v_{d,\mathrm{Ox},q,0} = \dot{m}_{\mathrm{Ox},q,l,0}/(\rho_{\mathrm{Ox},q,l,0}A_{\mathrm{Ox},q,l,0}) \tag{8b}$$

The total mass flow rate of the liquid propellant at the injection is the sum of the partial mass flow rates:

$$\dot{m}_{F,l,0} = \sum_{p=1}^{\mathrm{NF}} \sum_{i=1}^{I} \dot{m}_{F,p,l,i,0} \tag{9a}$$

$$\dot{m}_{\mathrm{Ox},l,0} = \sum_{q=1}^{\mathrm{NO}} \sum_{i=1}^{J} \dot{m}_{\mathrm{Ox},q,l,j,0} \tag{9b}$$

The partial mass flow rates of each propellant are calculated from the volume fractions of each size class from the given Rosin–Rammler distribution, multiplied by the total mass flow rate. In the same way, the injection areas of each liquid propellant are calculated by multiplying the volume fractions of each size class by the total injection area.

The fuel/oxidizer (F/O) premixed equivalence ratio and the F/O total equivalence ratio are expressed as

$$\Phi_P = \frac{f_P}{f_s} = \frac{1}{f_s}\frac{\dot{m}_{F,g,0}}{\dot{m}_{\mathrm{Ox},g,0}} \tag{10a}$$

$$\Phi_T = \frac{f_T}{f_s} = \frac{1}{f_s}\frac{\dot{m}_{F,g,0} + \dot{m}_{F,l,0}}{\dot{m}_{\mathrm{Ox},g,0} + \dot{m}_{\mathrm{Ox},l,0}} \tag{10b}$$

where Φ_P and Φ_T are the premixed equivalence ratio and the total equivalence ratio, respectively, and f_P, f_T, and f_s are the premixed, total, and stoichiometric mixture ratios, respectively. The partial mixture ratio f_P is the ratio of gaseous fuel mass flow rate and the gaseous oxidizer flow rate entering the chamber. The total mixture ratio f_T is the ratio of total gas and liquid fuel to the total gas and liquid oxidizer entering the chamber.

The liquid jet breakup distance is neglected, and, consequently, it is assumed that the droplets are formed close to the injector plate. The droplets enter the hot gas mixture, then are heated and vaporize. The total mass flow rate of gas at injection, $\dot{m}_{g,0}$, is given by

$$\dot{m}_{g,0} = \dot{m}_{F,g,0} + \dot{m}_{\mathrm{Ox},g,0} \tag{11}$$

where $\dot{m}_{F,g,0}$ and $\dot{m}_{\mathrm{Ox},g,0}$ are the mass flow rates of gaseous fuel and gaseous oxidizer, respectively, at the injection section. In the macroscale, i.e., away from the droplets, it is considered that fuel and oxidizer react instantaneously to form products.

The masses of liquid fuel and liquid oxidizer in a given chamber section can be written in terms of the diameters of the droplets:

$$\dot{m}_{F,l,i} = \sum_{p=1}^{\mathrm{NF}} \dot{m}_{F,p,l,i,0}\frac{\rho_{F,p,l,i}}{\rho_{F,p,l,i,0}}\left(\frac{D_{F,p,i}}{D_{F,p,i,0}}\right)^3 \tag{12a}$$

$$\dot{m}_{\mathrm{Ox},l,j} = \sum_{q=1}^{\mathrm{NO}} \dot{m}_{\mathrm{Ox},q,l,i,0}\frac{\rho_{\mathrm{Ox},q,l,j}}{\rho_{\mathrm{Ox},q,l,j,0}}\left(\frac{D_{\mathrm{Ox},q,l,j}}{D_{\mathrm{Ox},q,l,j,0}}\right)^3 \tag{12b}$$

where $D_{F,p,i}$ is the diameter of the p-fuel droplet of the size class I and $D_{\mathrm{Ox},q,j}$ is the diameter of a q-oxidizer droplet of the size class j. Differentiating Eqs. (12a) and (12b) with respect to x and considering the thermal expansion of droplets, it follows that

$$\dot{m}'_{F,l,i} = \sum_{p=1}^{\mathrm{NF}}\left(\frac{3\dot{m}_{F,p,l,i}}{D_{F,p,i}}D'_{F,p,i} + \frac{\dot{m}_{F,p,l,i}}{\rho_{F,p,l,i}}\frac{\mathrm{d}\rho_{F,p,l,i}}{\mathrm{d}T_{F,p,l,i}}T'_{F,p,l,i}\right) \tag{13a}$$

$$\dot{m}'_{\mathrm{Ox},l,j} = \sum_{q=1}^{\mathrm{NO}}\left(\frac{3\dot{m}_{\mathrm{Ox},q,l,j}}{D_{\mathrm{Ox},q,j}}D'_{\mathrm{Ox},q,j} + \frac{\dot{m}_{\mathrm{Ox},q,l,j}}{\rho_{\mathrm{Ox},q,l,j}}\frac{\mathrm{d}\rho_{\mathrm{Ox},q,l,j}}{\mathrm{d}T_{\mathrm{Ox},q,l,j}}T'_{\mathrm{Ox},q,l,j}\right) \tag{13b}$$

In Eqs. (13a) and (13b) the first term on the right side is positive during expansion of the droplet and the second is negative because the liquid density decreases with temperature. When the droplet attains an equilibrium temperature, assuming droplets with uniform temperature, the second term on the right side tends to zero.

The derivative of the droplet diameter along the chamber, $\mathrm{d}D/\mathrm{d}x$, is obtained from the transient evaporation theory of Chin and Lefebvre [14]. Following their formulation, Eqs. (13a) and (13b) can be rewritten in terms of droplet diameters:

$$D'_{F,p,i} = -\frac{2\dot{m}_{v,F,p,i}}{\pi\rho_{F,p,l,i}v_{d,F,p,i}D^2_{F,p,i}} - \frac{D_{F,p,i}}{3\rho_{F,p,l,i}}\frac{\mathrm{d}\rho_{F,p,l,i}}{\mathrm{d}T_{F,p,l,i}}T'_{F,p,l,i} \tag{14a}$$

$$D'_{\mathrm{Ox},q,j} = -\frac{2\dot{m}_{v,\mathrm{Ox},q,j}}{\pi\rho_{\mathrm{Ox},q,l,j}v_{d,\mathrm{Ox},q,j}D^2_{\mathrm{Ox},q,j}} - \frac{D_{\mathrm{Ox},q,j}}{3\rho_{\mathrm{Ox},q,l,j}}\frac{\mathrm{d}\rho_{\mathrm{Ox},q,l,j}}{\mathrm{d}T_{\mathrm{Ox},q,l,j}}T'_{\mathrm{Ox},q,l,j} \tag{14b}$$

where $\dot{m}_v$ is the droplet vaporization rate, given by

$$\dot{m}_v = \frac{\pi D\lambda_{g,r}Nu_0}{C_{\mathrm{pg},r}}\ell_n(1 + B_M) \tag{15}$$

and $l_{g,r}$ and $C_{\mathrm{pg},r}$ are, respectively, the thermal conductivity and specific heat of the mixture of propellant vapor and combustion products, calculated at a reference average temperature T_r, and $B_M = Y_s/(1 - Y_s)$.

D. Momentum Balances

A balance of the momentum fluxes along the chamber yields

$$P_{\mathrm{inj}} + (\rho_g v_g^2)_{\mathrm{inj}} + \left(\frac{\dot{m}_{F,l}}{A_c}v_{d,F}\right)_{\mathrm{inj}} + \left(\frac{\dot{m}_{\mathrm{Ox},l}}{A_c}v_{d,\mathrm{Ox}}\right)_{\mathrm{inj}} = P_f + (\rho_g v_g^2)_f \tag{16}$$

where the subscripts inj and f denote conditions at the injection and at the end of vaporization, respectively. Considering that $\rho_g v_g^2 = \gamma P M^2$, where g is the gas mixture specific heats ratio, ρ_g is the gas mixture density, v_g is the gas mixture velocity, and M is the flow Mach number, the following expression can be obtained for the pressure at the end of vaporization:

$$P_f = \frac{P_{\mathrm{inj}}(1 + \gamma_{\mathrm{inj}}M^2_{\mathrm{inj}}) + [(\dot{m}_{F,l}/A_c)v_{d,F}]_{\mathrm{inj}} + [(\dot{m}_{\mathrm{Ox},l}/A_c)v_{d,\mathrm{Ox}}]_{\mathrm{inj}}}{1 + \gamma_f M_f^2} \tag{17}$$

In general, in rocket combustion chambers,

$$M_{\mathrm{inj}} \ll 1$$

$$M_f \ll 1, \quad \text{and} \quad \left(\frac{\dot{m}_{F,l}}{A_c}v_{d,F}\right)_{\mathrm{inj}} + \left(\frac{\dot{m}_{\mathrm{Ox},l}}{A_c}v_{d,\mathrm{Ox}}\right)_{\mathrm{inj}} \ll P_{\mathrm{inj}}$$

consequently, $P_f \cong P_{\mathrm{inj}}$, and pressure variations along the chamber can be neglected.

The droplet accelerations are obtained using Newton's second law:

$$v'_{d,F,p,i} = \frac{3C_{D,F,p,i}\rho_g(v_g - v_{d,F,p,i})|v_g - v_{d,F,p,i}|}{4\rho_{F,p,l,i}v_{d,F,p,i}D_{F,p,i}} \tag{18a}$$

$$v'_{d,\mathrm{Ox},q,j} = \frac{3C_{D,\mathrm{Ox},q,j}\rho_g(v_g - v_{d,\mathrm{Ox},q,j})|v_g - v_{d,\mathrm{Ox},q,j}|}{4\rho_{\mathrm{Ox},q,l,j}v_{d,\mathrm{Ox},q,j}D_{\mathrm{Ox},q,j}} \tag{18b}$$

where C_D is calculated by the Wiegand [17] correlation that includes

the effects of aerodynamic deformation:

$$C_D \cong 0.28 + \frac{21}{Re_d} + \frac{6}{\sqrt{Re_d}} + We(0.2319 - 0.1579\log Re_d + 0.0471\log^2 Re_d - 0.0042\log^3 Re_d) \quad (19)$$

valid for $5 \le Re_d \le 2000$, where $We = \rho_g D v_{\text{rel}}^2/\tau_l$.

The gas mixture density is given by $\rho_g = P_g \bar{M}_g/(R_0 T_g)$, where P_g is the gas pressure, $\bar{M}_g$ is the molar mass of the gas mixture and R_0 is the universal gas constant (8.3145 kJ/kmol · K). Differentiating ρ_g gives

$$\rho'_g = \rho_g\left(\frac{1}{\bar{M}_g}\frac{\mathrm{d}\bar{M}_g}{\mathrm{d}T_g} - \frac{1}{T_g}\right)T'_g \quad (20)$$

The area occupied by the gas mixture along the chamber is $A_g = A_c - (A_{F,l} + A_{\text{Ox},l})$ where A_c is the internal section area of the combustion chamber and $A_{F,l}$ and $A_{\text{Ox},l}$ are the sum of all transverse areas of the fuel and oxidizer droplets, respectively, at position x. Differentiating A_g gives

$$A'_g = -A'_{F,l} - A'_{\text{Ox},l} \quad (21)$$

Differentiating the gas velocity equation $v_g = \dot{m}_g/(\rho_g A_g)$, substituting Eq. (20), and reordering yields

$$v'_g = v_g\left(\frac{\dot{m}'_g}{\dot{m}_g} - \frac{A'_g}{A_g}\right) - v_g\left(\frac{1}{\bar{M}_g}\frac{\mathrm{d}\bar{M}_g}{\mathrm{d}T_g} - \frac{1}{T_g}\right)T'_g \quad (22)$$

E. Energy Balance

Temperature variations of droplets are obtained from energy balances which yield

$$T'_{F,p,l,i} = \frac{\dot{Q}_{\text{rad},d,F,p,i} + \dot{Q}_{\text{conv},d,F,p,i} - \dot{Q}_{v,d,F,p,i}}{m_{d,F,p,i} v_{d,F,p,i} C_{pl,F,p,i}} \quad (23a)$$

$$T'_{\text{Ox},q,l,j} = \frac{\dot{Q}_{\text{rad},d,\text{Ox},q,j} + \dot{Q}_{\text{conv},d,\text{Ox},q,j} - \dot{Q}_{v,d,\text{Ox},q,j}}{m_{d,\text{Ox},q,j} v_{d,\text{Ox},q,j} C_{pl,\text{Ox},q,j}} \quad (23b)$$

where $\dot{Q}_{\text{rad},d}$ and $\dot{Q}_{\text{conv},d}$ are the heat flows by radiation and convection, respectively, from the hot gases to the droplet, and $\dot{Q}_{v,d}$ is the vaporization heat flow of a representative droplet of a given size class. Radiation from the chamber wall to the droplets was neglected, because the gas temperature is much higher than the wall temperature. The heat flow by radiation to a single droplet is $\dot{Q}_{\text{rad},d} = \varepsilon_g \sigma A_d (T_g^4 - T_l^4)$ where $\sigma = 5.6704 \times 10^{-8}$ W/m^2 · K^4. The gas mixture emissivity was calculated using an expression given by Leckner [18] that is function of the combustion chamber characteristic length, gas temperature, partial pressure P_i(i= CO_2 or H_2O), and total pressure [12].

The convective heat flow to the droplet is given by $\dot{Q}_{\text{conv},d} = \tilde{h}^* A_d (T_g - T_l)$, where $\tilde{h}^*$ is the convection coefficient including blowing effects [19]. The vaporization heat flow is given by $\dot{Q}_v = \dot{m}_v h_{\text{fg}}$, where h_{fg} is dependent on temperature and pressure.

The vapor pressure P_v (kPa) of each propellant is calculated by Antoine's equation:

$$\log_{10} P_v = A - \frac{B}{T + C}, \qquad (T = K) \quad (24)$$

where A, B, and C are constants, shown on Table 1. These constants were obtained in [1], or derived from plots in [16].

The vaporization enthalpy h_{fg} is calculated from the Haggenmacher [20] equation, which is a combination of the Antoine and Clausius–Clapeyron equations:

$$h_{\text{fg}} = \frac{BR_v T^2 \log_{10} e}{(T + C)^2}\left[1 - \left(\frac{T_c}{T}\right)\left(\frac{P_v}{P_c}\right)\right]^{1/2} \text{ kJ/kg}, \qquad (T = K) \quad (25)$$

where B and C are the constants of Antoine's equation, R_v is the vapor constant, and T_c and P_c are the critical temperature and critical pressure, respectively, of propellants.

An energy balance for the gas phase inside an element volume gives the following expression for the gas temperature gradient:

$$T'_g = -\frac{1}{a_2}(a_1 + W_F + W_{\text{Ox}} + \dot{Q}'_{\text{conv},w} + \dot{Q}'_{\text{rad},w}) \quad (26)$$

with

$$W_F = \sum_{p=1}^{\text{NF}}\sum_{i=1}^{I}\Big[\dot{m}_{F,p,l,i}\Big(C_{pF,p,l,i}T'_{F,p,l,i} + v_{d,F,p,i}v'_{d,F,p,i}\Big) + \dot{m}'_{F,p,l,i}\Big(h_{F,p,l,i} + 0.5v^2_{d,F,p,i}\Big)\Big] \quad (27)$$

$$W_{\text{Ox}} = \sum_{q=1}^{\text{NO}}\sum_{i=1}^{I}\Big[\dot{m}_{\text{Ox},q,l,j}\Big(C_{p\text{Ox},q,l,j}T'_{\text{Ox},q,l,j} + v_{d,q,\text{Ox},j}v'_{d,\text{Ox},q,j}\Big) + \dot{m}'_{\text{Ox},q,l,j}\Big(h_{\text{Ox},q,l,j}\dot{m}'_{\text{Ox},q,l,j} + 0.5v^2_{d,\text{Ox},q,j}\Big)\Big] \quad (28)$$

$$a_1 = \dot{m}_g v_g^2\left[\frac{3\dot{m}'_g}{2\dot{m}_g} - \frac{A'_g}{A_g}\right] + \left[\dot{m}_g \Phi' \frac{\mathrm{d}h_g}{\mathrm{d}\Phi} + h_g \dot{m}'_g\right] \quad (29)$$

$$a_2 = \dot{m}_g\left[\frac{\mathrm{d}h_g}{\mathrm{d}T_g} - v_g^2\left(\frac{1}{\bar{M}_g}\frac{\mathrm{d}\bar{M}_g}{\mathrm{d}T_g} - \frac{1}{T_g}\right)\right] \quad (30)$$

where Φ is the local equivalence ratio of the gas mixture. Heat convection flow to the wall, $\dot{Q}_{\text{conv},w}$, and heat radiation flow from gas to the wall, $\dot{Q}_{\text{rad},w}$, are calculated, respectively, by the equations

$$\dot{Q}'_{\text{conv},w} = \hat{h}_g \pi D_c (T_g - T_{\text{wi}}) \quad (31a)$$

$$\dot{Q}'_{\text{rad},w} = \varepsilon_g \sigma \pi D_c (T_g^4 - T_{\text{wi}}^4) \quad (31b)$$

where T_{wi} is the internal temperature of the chamber wall, D_c is the chamber internal diameter and $\hat{h}_g$ is the convection coefficient from the hot gases, which depends on fluid and flow properties.

The gas enthalpy h_g and its derivatives $\mathrm{d}h_g/\mathrm{d}T$ and $\mathrm{d}h_g/\mathrm{d}\Phi$ can be calculated from the equilibrium composition of the gas mixture for values of T, P, and Φ specified. To calculate these derivatives and other properties, an equilibrium code was written for $C_xH_yO_zN_t$ fuels and N_pO_q oxidizers, including up to 11 species: CO_2, CO, H_2O, H_2, O_2, N_2, O, H, OH, NO, and N. In the simulations the thermodynamic properties were dependent on temperature and were obtained from CHEMKIN database [21].

F. Input Data for Simulations

The system of differential and auxiliary equations obtained, including Eqs. (4–31), was solved using the data shown on Table 2, for single component hydrazines, and data on Table 3, for hydrazine mixtures. These data were based on a 200 N bipropellant thruster using MMH and NTO, designed with a characteristic length

Table 2 Data for simulation of chambers using single hydrazines

$P_c = 10$ atm	$T_{g,0} = 800$ K	$\dot{m}_{F,l,0} = 11.43$ g/s	$q_F = 2.5(-)$
$P_a = 0$ atm	$T_\infty = 300$ K	$\dot{m}_{\text{Ox},l,0} = 28.57$ g/s	$q_{\text{Ox}} = 2.5(-)$
$A_{F,l,0} = 15$ mm^2	$T_{F,l,0} = 280$ K	$\dot{m}_{\text{Ox},g,0} = 2.857$ g/s	$D_{32,F} = 50$ μm
$A_{\text{Ox},l,0} = 35$ mm^2	$T_{\text{Ox},l,0} = 280$ K	$\dot{m}_{F,g,0} = 2.428$ g/s	$D_{32,\text{Ox}} = 50$ μm

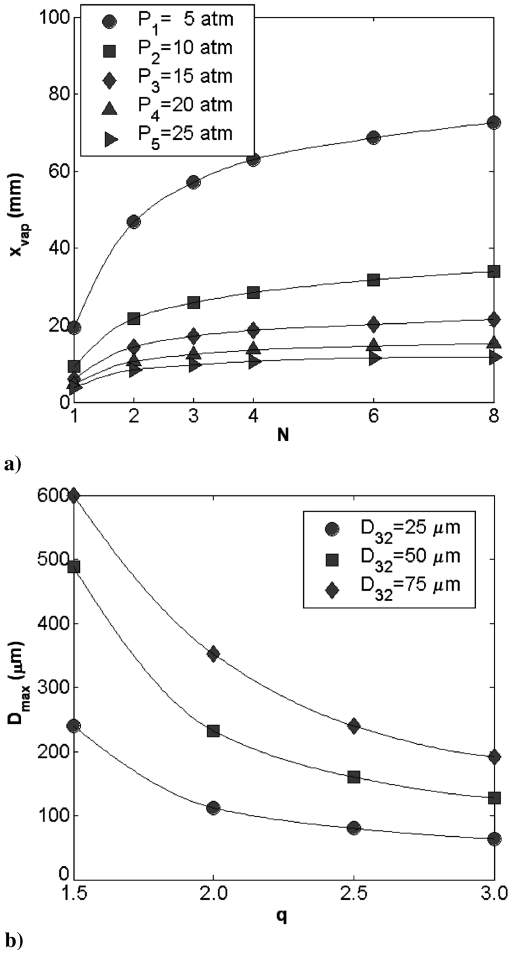

Fig. 4 a) Influence of number of size classes and pressure on vaporization lengths, x_{vap}. b) Influence of Rosin–Rammler parameters for MMH burning with NTO.

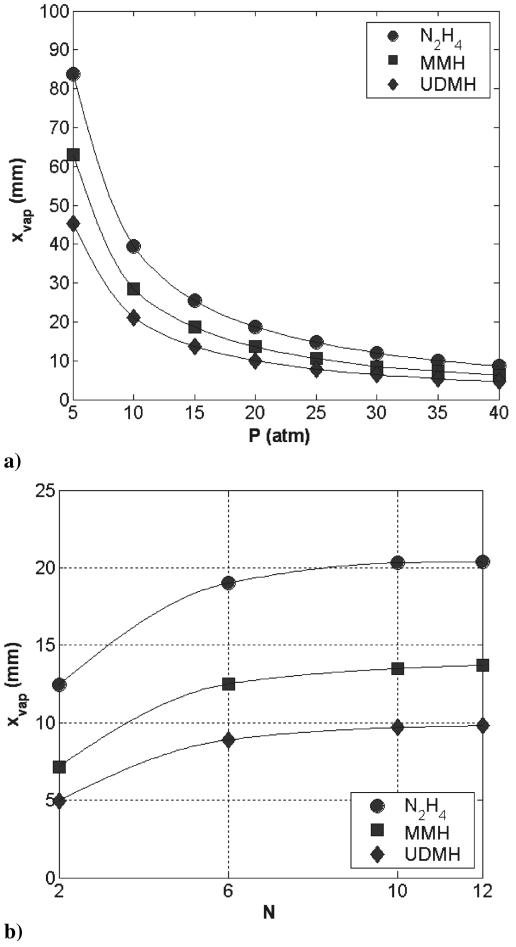

Fig. 5 a) Influence of pressure on complete vaporization length of hydrazines burning with NTO, $N = 4$ classes. b) Influence of number of droplet size classes on complete vaporization lengths of hydrazine fuels burning with NTO, $P = 25$ atm.

$L^* \approx 1.2$ m, chamber diameter $D_c = 40$ mm, chamber wall material Inconel 600, and wall thickness 3 mm [22].

Vacuum conditions were considered, with no convective heat transfer from external walls, because the 200 N thruster was tested in a vacuum chamber. Lower wall temperatures would be attained if external convection heat transfer were significant. It was assumed that fixed fractions of the initial flow rates of each liquid propellant, $\dot{m}_{\mathrm{Ox},g,0} = 0.1\dot{m}_{\mathrm{Ox},l,0}$ and $\dot{m}_{F,g,0} = 0.85\dot{m}_{\mathrm{Ox},g,0}$, vaporized instantaneously just after entering the chamber, to originate a premixed flow of gases near the injection plate.

Bipropellant systems using MMH/NTO, N_2H_4/NTO, and UDMH/NTO were simulated with total mass flow rates 45.29 g/s, total mass flow rates of liquid propellants 40 g/s, initial fuel-oxidizer mass mixture ratio of liquid propellants 0.4, and initial mass mixture ratio of gaseous propellants 0.85.

Bipropellant systems using N_2H_4–MMH and N_2H_4–UDMH mixtures burning with NTO were simulated with total mass flow rates 89.25 g/s, total mass flow rate of liquid propellants 80 g/s, initial mass mixture ratio for all liquid propellants 0.6, and initial mass mixture ratio for all gaseous propellants 0.85. In a few cases other values were used, but they are mentioned in the text or in the figures' legends. Because complete thermodynamic data for all hydrazine mixtures were not available, they were simulated assuming the components were injected separately, with mass percentages of N_2H_4 varying from 20 to 80%. Results show the influence of the mass percentage of N_2H_4 on the vaporization lengths of droplets, x_{vap}.

The critical pressures of N_2H_4, MMH, and UDMH are 145.00, 79.30, and 59.81 atm, respectively, therefore the results presented were limited to subcritical pressures.

III. Analysis and Discussion

The vaporization length, x_{vap}, is an important parameter for determination of the length of a rocket combustion chamber, whereas the temperature profiles are important for performance determination (calculate nozzle exit velocities), cooling design and for safety reasons, because material yield strength varies with temperature.

Results shown in Figs. 5–11 were obtained for bipropellant systems N_2H_4/NTO, MMH/NTO, and UDMH/NTO, and results shown in Fig. 12–14 were obtained for bipropellant systems using hydrazine mixtures N_2H_4–MMH and N_2H_4–UDMH burning with NTO.

Figure 5a compares the influence of chamber pressure, P, on droplet vaporization length, x_{vap}. The plots show that when P increases, x_{vap} decreases. This can be explained by the increase on vaporization rates with pressure, as previously showed by Chin and Lefebvre [14,15].

Results in Fig. 5a were obtained with four size classes (each class with a characteristic diameter). As already mentioned, the choice of an appropriate number of size classes is important because a large number of classes can increase significantly the computation time, but, on the other hand, a small number of classes can produce significant errors on estimates of the vaporization lengths. It is seen that vaporization lengths tend to asymptotic values for increasing numbers of size classes, depending on pressure.

It is observed in Fig. 5a that vaporization distances for N_2H_4 droplets are larger than for MMH and UDMH, because the N_2H_4 boiling point (113.5°C) is much higher than MMH (90.9°C) and UDMH (63°C) boiling points, and, consequently, N_2H_4 droplets require more time for attaining an equilibrium temperature.

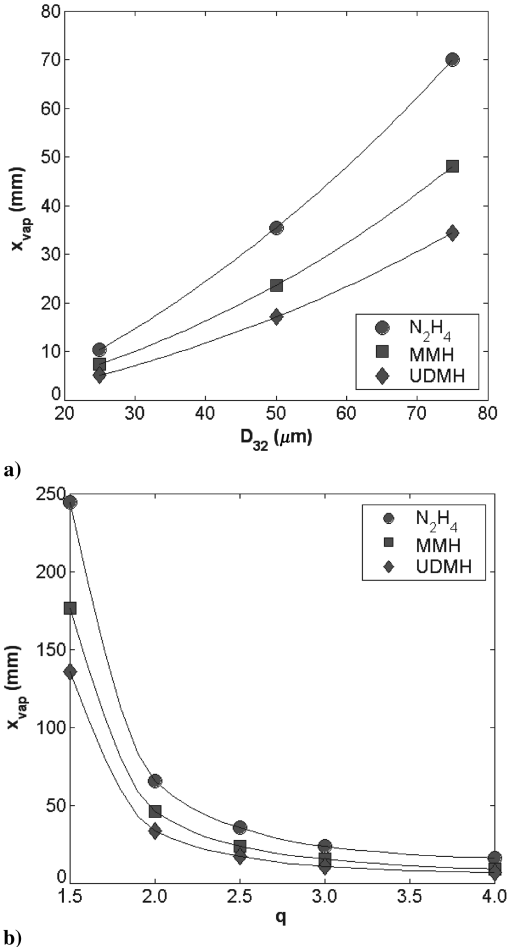

Fig. 6 (a) Influence of Sauter mean diameter on complete vaporization lengths of hydrazine fuels burning with NTO, $q = 2.5$. b) Influence of parameter of Rosin–Rammler distribution on complete vaporization lengths of hydrazine fuels burning with NTO, $D_{32} = 50$ μm.

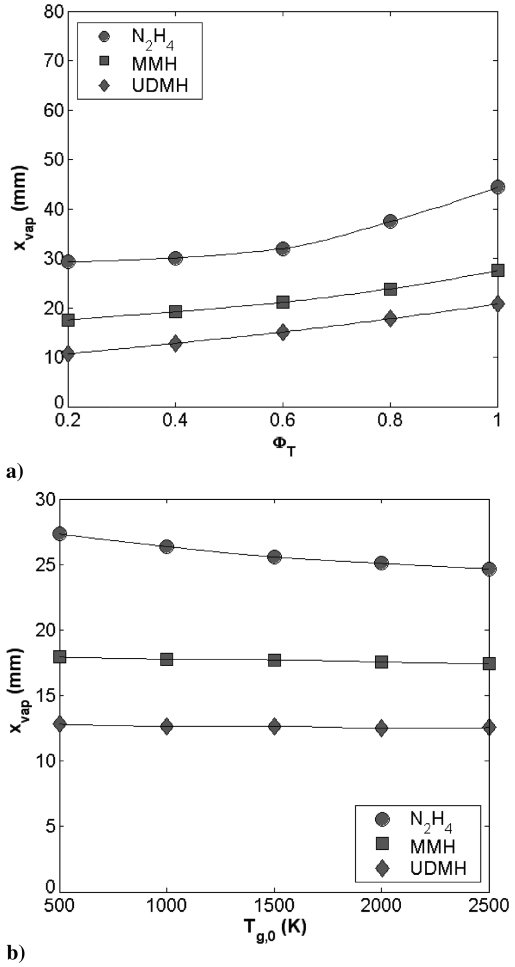

Fig. 7 a) Influence of total equivalence ratio on complete vaporization length for hydrazines burning with NTO, $N = 8$ classes, $P = 20$ atm. b) Influence of initial gas temperature on complete vaporization length for hydrazines burning with NTO, $N = 8$ classes, $P = 20$ atm.

Figure 5b compares the influence of the number of size classes, N, or number of representative diameters of droplets, on complete vaporization distance of the three hydrazines. It is again observed that N_2H_4 has a larger vaporization distance than the other two hydrazines. Figure 5b shows that the vaporization distance approaches a constant value as the number of size classes increase. For $N \geq 8$ and for a pressure of 25 atm, the vaporization length does not vary significantly.

Figures 6a and 6b show the influence of Rosin–Rammler parameters, D_{32} and q, respectively, on vaporization distances of hydrazines. The plots were obtained for eight size classes and a chamber pressure of 15 atm. As expected, for increasing diameters D_{32}, the vaporization length increases. As q increases, the vaporization distance decreases in exponential form, because the spray distribution becomes more uniform and the droplets get similar sizes.

Figure 7a shows the influence of total equivalence ratio, Φ_T, on complete vaporization distance of hydrazines. In this case the mass flow rate for each fuel is given by $\dot{m}_{F,0} = \dot{m}_{F,g,0} + \Phi_T f_s \dot{m}_{\mathrm{Ox},0}$, where f_s is the stoichiometric mass ratio and $\dot{m}_{F,g,0} = 0.85\dot{m}_{\mathrm{Ox},g,0}$. For this case, the vaporization lengths increase as a consequence of the larger mass flow rates of fuel injected.

Figure 7b shows the influence of the initial gas flow temperature, T_{g0}, on complete vaporization distance of hydrazines. It is observed that T_{g0} does not affect significantly the vaporization length, in the temperature range 500–2500 K. This occurs because the premixed gases react rapidly just after they enter the chamber, attaining a combustion temperature that depends basically on local mixture ratio and chamber pressure.

The results showed in Figs. 8–12 were obtained for a pressure of 25 atm and four droplet size classes. Representative droplet diameters of the size classes were 32, 64, 98, and 133 μm. Only the larger droplets, with diameter 133 μm, were used to compare the evolution of the various parameters along the combustion chamber.

Figure 8a shows the evolution of the nondimensional diameter, D/D_0, along the combustion chamber. It is observed a preheating region where there is a significant thermal expansion of droplets. The length of this region increases when the pressure increases and diminishes when the temperature is higher, in agreement with results from [14,23].

The length of the region of thermal expansion of the liquid depends, besides pressure, on the initial liquid temperature, i.e., the closer the entrance temperature is to the boiling temperature, the shorter the preheating zone. N_2H_4 droplets present a larger vaporization length than other hydrazines because of their longer preheating time, caused by the larger difference between boiling temperature and entrance temperature, as already verified in Fig. 5a. N_2H_4 presents a maximum increase of droplet diameter of approximately 18% due to liquid thermal expansion, whereas MMH and UDMH present maximum expansions of about 5%.

Figure 8b shows the evolution of droplet velocity, v_d, and the gas velocity, v_g, along the combustion chamber. The injection velocities for each hydrazine are slightly different due to their different liquid densities. The droplet final velocities approach the gas velocity due to drag effects. N_2H_4 velocities are lower than MMH and UDMH velocities, because the liquid velocity varies inversely with the liquid density. The gas velocity increases until the complete vaporization of droplets.

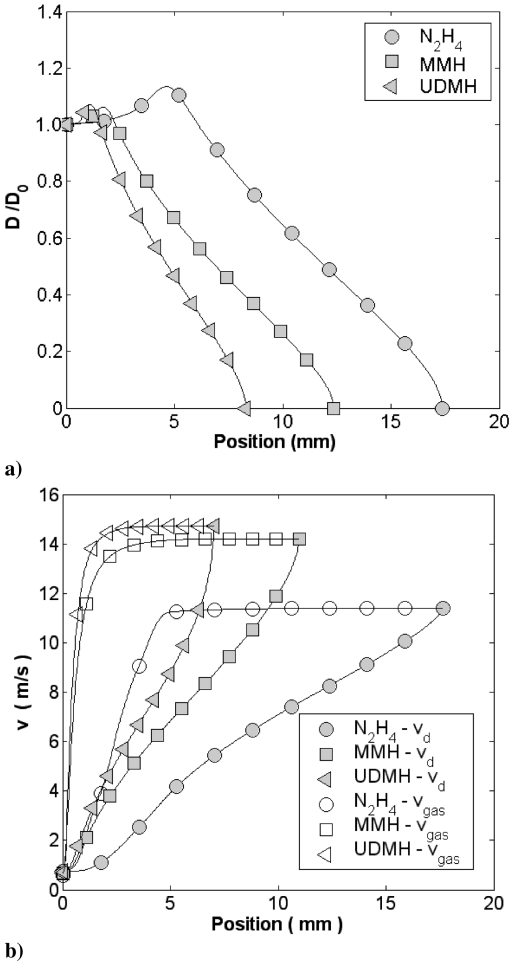

Fig. 8 a) Nondimensional diameter of droplets along a bipropellant combustion chamber for hydrazines burning with NTO, $\phi_d = 133$ μm. b) Gas velocity and droplet velocity along a bipropellant combustion chamber for hydrazines burning with NTO, $\phi_d = 133$ μm.

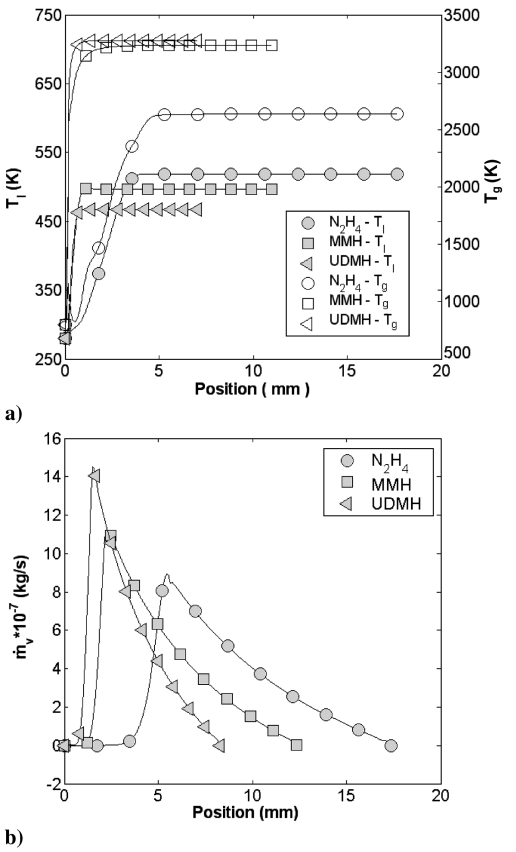

Fig. 9 a) Droplet temperature and gas temperature along a bipropellant combustion chamber for hydrazines burning with NTO, $\phi_d = 133$ μm. b) Vaporization rate along a bipropellant combustion chamber for hydrazines burning with NTO, $\phi_d = 133$ μm.

Figure 9a shows the liquid temperature and the gas temperature along the combustion chamber. The droplet temperature increases up to the equilibrium temperature at the chamber pressure. The gas temperature of N_2H_4 presents a small decrease near the injection due to the higher boiling temperature compared with other hydrazines. The equilibrium temperature of N_2H_4 droplets is larger than the equilibrium temperatures of MMH and UDMH droplets whereas the gas temperature for N_2H_4 is lower than for the other hydrazines.

Figure 9b shows the variation of the rate of vaporization of liquid propellants along the combustion chamber. The rate of vaporization increases during the droplet preheating period and attains a maximum when the droplet reaches the equilibrium temperature at the chamber pressure, and, after, decreases until the complete vaporization of droplets. The rate of vaporization is directly proportional to the droplet diameter and increases with droplet expansion.

Figures 10a and 10b show the heat losses by convection and radiation from the gas mixture to the droplets along the combustion chamber. It is observed that heat transfer by convection is approximately 60 times larger than radiation heat transfer. Heat losses increase during the preheating period up to a maximum when the liquid temperature is close to the equilibrium temperature and decrease until the complete vaporization of droplets.

Figure 11 shows the nondimensional surface area of droplets, D^2/D_0^2, as function of time. During the preheating of droplets, the droplets present thermal expansion. The preheating phase lasts longer than the vaporization period without droplet heating, as also verified in studies of Borman and Ragland [23]. It is seen that the D^2 law is approximately valid after the preheating phase. The complete vaporization time is relatively short, of order 10^{-3} s.

Figure 12 shows the influence of mass percentage of N_2H_4 on vaporization lengths of N_2H_4 and MMH droplets in the system N_2H_4–MMH/NTO. Because it is considered in the analysis the injection of two fuels separately, there are two fuel vaporization distances. If pressure increases, the vaporization length decreases, as seen before for single hydrazines. Mixtures with higher mass percentages of N_2H_4 present larger vaporization lengths, because $T_{b,N_2H_4} = 113.5°C > T_{b,MMH} = 90.9°C > T_{b,UDMH} = 63°C$. In all bipropellant systems simulated using hydrazine "mixtures," the N_2H_4 vaporization lengths are larger than the MMH vaporization lengths.

Figure 13 shows the influence of mass percentage of N_2H_4 on vaporization lengths of N_2H_4 and UDMH droplets in the system N_2H_4–UDMH/NTO. Similarly to the preceding case, N_2H_4 droplets have larger vaporization lengths than UDMH droplets.

Figure 14 shows the influence of mass percentage of N_2H_4 in the N_2H_4–MMH and N_2H_4–UDMH bipropellant systems on maximum gas temperature, $T_{g,\max}$. It is observed that larger N_2H_4 percentages yield larger maximum gas temperatures, when $\Phi_g \approx 1$, and that the maximum gas temperature increases with pressure.

It can be seen that vaporization lengths of N_2H_4–MMH mixtures are larger than vaporization lengths of N_2H_4–UDMH mixtures. Because vaporization lengths of N_2H_4 are larger than MMH or UDMH in the case of hydrazine mixtures, they should be used to estimate the chamber length. When the mass percentage of N_2H_4 increases from 20 to 80%, the vaporization lengths of N_2H_4 increase about 20%, from, approximately, 60 to 72 mm, which can lead to a corresponding increase in the chamber weight, a relevant factor in rocket propulsion systems.

It should be noted that species with different volatilities within a multicomponent droplet will vaporize at different rates during the

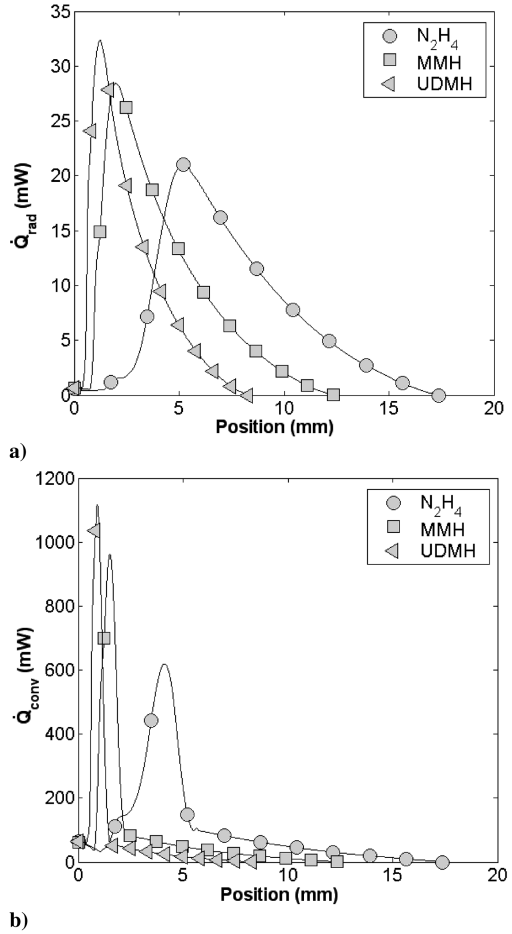

Fig. 10 a) Heat losses by radiation from gas to fuel droplets, along bipropellant combustion chamber for hydrazines burning with NTO, $\phi_d = 133$ μm. b) Heat losses by convection from gas to fuel droplets, along bipropellant combustion chamber for hydrazines burning with NTO, $\phi_d = 133$ μm.

droplet lifetime. However, because the thermodynamic properties of the hydrazine mixtures are not known for all compositions it was assumed that the droplet components behave independently.

IV. Conclusion

The performances of hydrazine fuels burning with NTO in a bipropellant rocket combustion chamber were compared using a one-dimensional mathematical model. Systems using single hydrazines (N_2H_4, MMH, UDMH) and hydrazine mixtures (MMH/N_2H_4 and UDMH/N_2H_4) were simulated with total mass

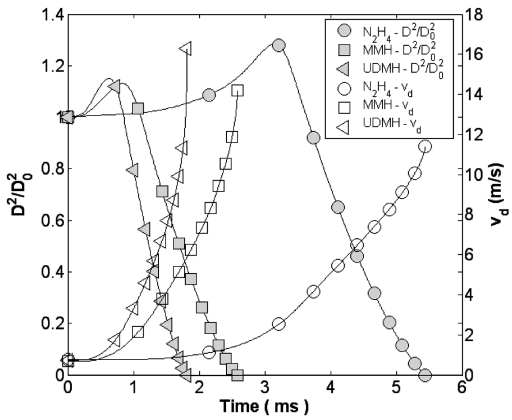

Fig. 11 Nondimensional surface area and droplet velocity versus time, t, for hydrazines burning with NTO, $\phi_d = 133$ μm.

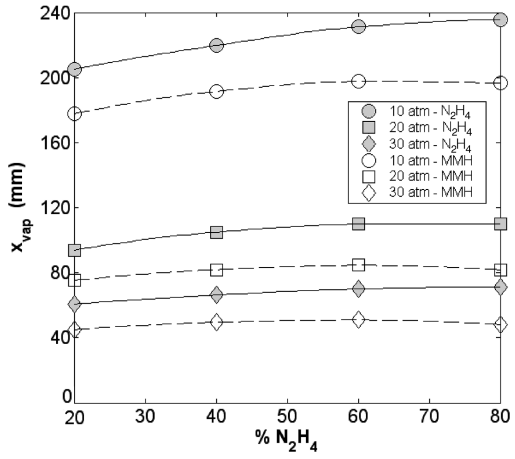

Fig. 12 Influence of mass percentage of N_2H_4 on vaporization length of N_2H_4 and MMH droplets in bipropellant system N_2H_4–MMH/NTO.

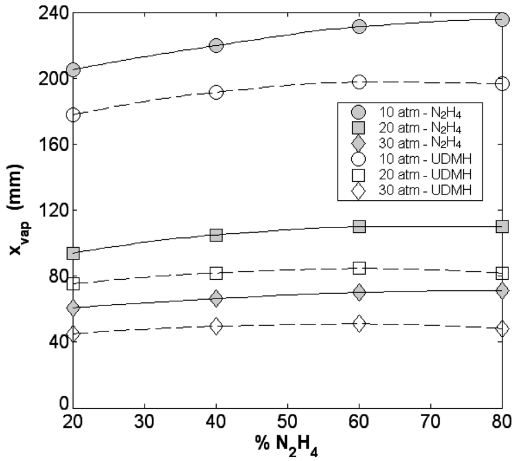

Fig. 13 Influence of mass percentage of N_2H_4 on vaporization lengths of N_2H_4 and UDMH droplets in bipropellant system using N_2H_4–UDMH/NTO.

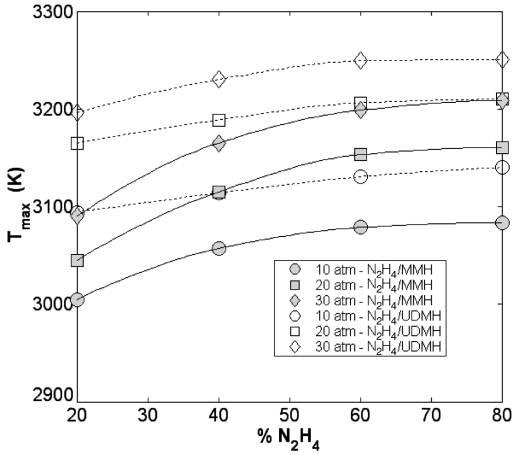

Fig. 14 Influence of mass percentage of N_2H_4 on maximum gas temperature of bipropellant systems using N_2H_4–MMH and N_2H_4–UDMH mixtures.

flow rates of 45.29 g/s and 89.25 g/s, respectively, in a chamber with diameter 40 mm.

It was assumed that combustion and turbulent mixture processes are controlled by droplet vaporization, and that fuel and oxidizer droplet diameters follow Rosin–Rammler distribution functions, but with a finite number of diameters. The effects of drag, thermal

expansion, transient vaporization, convection, and radiation to the droplets and heat losses to the chamber walls were considered. The influences of chamber pressure, equivalence ratio, initial gas temperature, number of size classes of droplets, Sauter mean diameter, and Rosin–Rammler distribution parameters on the distance for complete vaporization of drops were analyzed. Profiles of normalized diameters, temperatures, velocities, heat losses, vaporization rates, and other flow properties along the chamber were described.

It was observed that in bipropellant systems using single hydrazines, $x_{\mathrm{vap},N_2H_4} > x_{\mathrm{vap,MMH}} > x_{\mathrm{vap,UDMH}}$, for all cases considered. For the input conditions considered it was verified that vaporization lengths of single hydrazines decrease with increasing pressures up to 40 atm, remaining approximately constant for higher pressures.

For a pressure of 25 atm, a number of eight droplet diameter classes can represent satisfactorily the spray, whereas for lower pressures, four droplet size classes can be used. Vaporization lengths increase for larger Sauter mean diameters and decrease for larger distribution function parameters q. The vaporization length is approximately constant for q larger than 3.5, considering $D_{32} = 50\ \mu$m.

The preheating time of N_2H_4 droplets is larger than for MMH and UDMH droplets, with diameter expansion of about 18% for N_2H_4 droplets and about 5% for MMH and UDMH droplets, during the preheating phase. Convective heat transfer to the droplets is much larger than heat transfer by radiation. Initial velocities of hydrazines are approximately the same, depending mainly on injection temperatures, wheras the final velocities of N_2H_4 droplets are lower than final velocities of MMH and UDMH droplets.

Vaporization rates of hydrazines increase during preheating phase up to a maximum when droplets attain an equilibrium temperature. From this point on the vaporization rates decrease continuously, following approximately a D^2-law, until complete vaporization.

In bipropellant systems using hydrazine mixtures N_2H_4/UDMH and N_2H_4/MMH, the mass percentage of N_2H_4 does not affect significantly the vaporization lengths, but higher hydrazine mass percentages increase the gas temperatures. Vaporization lengths are larger for N_2H_4/MMH mixtures than for N_2H_4/UDMH mixtures, whereas maximum gas temperatures in N_2H_4/MMH mixtures are lower than in N_2H_4/UDMH mixtures.

It should be noted that species with different volatilities within a multicomponent droplet will vaporize at different rates during the droplet lifetime. However, because the thermodynamic properties of the hydrazine mixtures are not known for all compositions it was assumed that the droplet components behaved independently.

Acknowledgment

The authors acknowledge National Council for Research and Technological Development/Brazil for the grant of a scholarship to the first author.

References

[1] Schmidt, E. W., *Hydrazine and its Derivates-Preparation, Properties, Applications*, John Wiley & Sons, New York, 1984.

[2] Kuo, K. K., *Principles of Combustion*, John Wiley & Sons, New York, 1986.

[3] Bracco, F. B., "Theoretical Analysis of Stratified, Two-Phase Wankel Engine Combustion," *Combustion Science and Technology*, Vol. 8, No. 1, 1973, pp. 69–84.

[4] Dickinson, D. R., and Marshall, W. R., Jr., "Rates of Evaporation of Sprays," *AIChE Journal*, Vol. 14, No. 4, 1968, pp. 541–552.

[5] Hersch, M., "A Mixing Model for Rocket Engine Combustion," NASA TN D-2881, 1965.

[6] Krioukov V. G., Iskhakova, R. L., Niwa, M., Dregalin, A. F., and Jukova, I. K., "Mathematical Modeling of Two-Phase Reacting Flow in Supersonic Nozzle," *Proceedings of the 17th International Congress of Mechanical Engineering, COBEM 2003* [CD-ROM], Rio de Janeiro, 2003.

[7] Law, C. K., "Theory of Monodisperse Spray Vaporization in Adiabatic and Isorthermal Systems," *International Journal of Heat and Mass Transfer*, Vol. 18, No. 11, 1975, pp. 1285–1292.

[8] Priem, R. J., and Heidmann, M. F., "Propellant Vaporization as a Design Criterion for Rocket-Engine Combustion Chambers," NASA TR R-67, 1960.

[9] Spalding, D. B., "A One-Dimensional Theory of Liquid Fuel Rocket Combustion," Ames Research Center (NASA) TR No. 20-175, Current Paper No. 445, 1959.

[10] Turns, S. R., and Faeth, G. M., "A One-Dimensional Model of a Carbon-Black Slurry-Fueled Combustor," *Journal of Propulsion and Power*, Vol. 1, No. 1, 1985, pp. 5–10.

[11] Williams, F. A., *Combustion Theory*, 2nd ed., Addison Wesley Longman, Reading, MA, 1985, Chap. 11.

[12] Valverde, C. A., "Mathematical Model of Bipropellant Combustion Chambers," M.Sc. Dissertation (in Portuguese), Instituto Nacional de Pesquisas Espaciais, SP, Brazil, 2004.

[13] Huzel, D. K., and Huang, D. H., *Modern Engineering for Design of Liquid-Propellant Rocket Engines*, Vol. 147, Progress in Astronautics and Aeronautics, AIAA, Washington, D.C., 1992.

[14] Chin, J. S., and Lefebvre, A. H., "Steady-State Evaporation Characteristics of Hydrocarbon Fuel Drops," *AIAA Journal*, Vol. 21, No. 10, Oct. 1983, pp. 1437–1443.

[15] Lefebvre, A. H., *Atomization and Sprays Combustion*, Hemisphere Publishing Corporation, New York, 1989.

[16] Linstrom, P. J., and Mallard, W. G., *NIST Chemistry WebBook*, NIST Standard Reference Database No. 69, National Institute of Standards and Technology, Gaithersburg, MD, (http://webbook.nist.gov), June 2005.

[17] Wiegand, H., Die Einwirkung eines ebenen strömungsfeldes auf frei bewegliche tropfen und ihren widerstandsbeiwert im Reynoldszahlenbereich von 50 bis 2000, Reihe: Fortschrittberichte VDI, 1987.

[18] Leckner, B., "Spectral and Total Emissivity of Water Vapor and Carbon Dioxide," *Combustion and Flame*, Vol. 19, No. 1, 1972, pp. 33–48.

[19] Zhou, L., *Theoretical and Numerical Modeling of Turbulent Gas Flows and Combustion*, CRC, Boca Raton, FL, 1993.

[20] Haggenmacher, J. E., "The Heat of Vaporization as a Function of Pressure and Temperature," *Journal of the American Chemical Society*, Vol. 68, No. 8, 1946, pp. 1633–1634.

[21] Kee, R. J., Rupley, F. M., Miller, J. A., Coltrin, M. E., Grcar, J. F., and Glarborg, P., *Chemkin Collection Release v. 3.7: Thermodynamic Data. Thermodynamic Property Database and the FITDAT Data-Fitting Utility* [CD-ROM], Reaction Design, San Diego, CA, 2002.

[22] Hinckel, J. N., Kozlov, A. A., Vicente de Moraes, F. J., and Cardoso, H. P., "Development of a 200 N Bipropellant Thruster," *Proceedings of the IX Brazilian Congress of Thermal Engineering and Sciences, ENCIT 2002*, [CD-ROM], Rio de Janeiro, 2002.

[23] Borman, G. L., and Ragland, K. W., *Combustion Engineering*, McGraw–Hill, New York, 1998.

C. Avedisian
Associate Editor